Surface Science 604 (2010) 893–897

Contents lists available at ScienceDirect

Surface Science

journal homepage: www.elsevier.com/ locate/susc

Experimental observation of the strong influence of crystal orientation on Electron Rutherford Backscattering Spectra

Maarten Vos [a,*], Koceila Aizel [a], Aimo Winkelmann [b]

[a] Research School of Physics and Engineering, Australian National University, Canberra ACT, Australia
[b] Max Planck Institute for Microstructure Physics, Halle (Saale), Germany

ARTICLE INFO

Article history:
Received 19 October 2009
Accepted 16 February 2010
Available online 3 March 2010

Keywords:
Elastic electron scattering
Kikuchi pattern
Electron Rutherford Backscattering

ABSTRACT

In Electron Rutherford Backscattering Spectroscopy (ERBS) energetic electrons (in our case up to 40 keV) impinge on a target and one measures the energy of elastically scattered electrons. This energy depends on the mass of the scattering atom, due to the recoil effect. This technique thus provides information about the sample composition. For single crystals the interaction of the projectile electron with the crystal potential modifies the angular intensity distribution of the scattered electrons. This leads, for example, to the well-known Kikuchi patterns. Here we investigate if such modified angular distribution has any influence on the intensity ratio of the observed elastic peaks in ERBS. Dramatic effects are found. Implications of these observations for quantitative surface analysis using energetic electrons are discussed.

© 2010 Elsevier B.V. All rights reserved.

1. Introduction

In recent years it has become obvious that the spectrum of elastically scattered electrons (momentum before scattering k_0, after scattering k_1), with incoming energy E_0 in the multiple keV range consists of several peaks due to scattering from atoms with different mass. The change in momentum of the scattered electron, $q = k_1 - k_0$, is reflected in an opposite change in momentum of the scattering atom. Due to this recoil momentum the scattering atom acquires kinetic energy ($q^2/2M$, M the atomic mass), and the energy of the electron is reduced by this amount. Because of this energy change the collision is sometimes described as quasi-elastic. The recoil energy is measurable for large q values only, that is, for large E_0 values and large scattering angles. Hydrogen can be separated from heavier elements for E_0 values over 1 keV [1–4], but resolving the contributions of heavier elements requires energies above 10 keV [5,6]. These experiments are often referred to as Electron Rutherford Backscattering Spectroscopy (ERBS) and open up new opportunities that were not considered in traditional elastic peak electron spectroscopy (EPES) as reviewed by Gergely [7].

Large-angle scattering events at high energies destroy the coherence of the backscattered electron wave with respect to the incident wave, as is seen by an extremely small Debye–Waller factor. This means that completely coherent reflection and diffraction effects can be usually neglected (such processes would typically result in spot diffraction patterns). However, this does not mean that the ERBS measurements are totally unaffected by diffraction effects. Both the incoming electrons *before* the incoherent backscattering event and the outgoing electrons *after* the incoherent backscattering event are influenced by strong coherent *forward* scattering. The diffraction of the outgoing electron wave by the lattice results in Kikuchi patterns observed in the angular distribution of the backscattered electrons (electron backscatter diffraction patterns) [8,9], while diffraction of the incoming electron wave is the basis of electron channeling effects [10]. This means that on the one hand the incident beam channeling modulates the probability that the electron is incoherently back-scattered from a target atom (independent of its outgoing direction), and on the other hand the electron backscatter diffraction has a large influence on the intensity distribution of the electrons leaving the crystal (independent of their incoming direction). The combination of both kinds of diffraction effects has dramatic influences on the observed relative intensity of different elements in an ERBS spectrum from crystalline targets, as we will demonstrate in this paper.

2. Experimental details

The experimental set-up was described in some detail in Ref. [6] and the geometry is sketched in Fig. 1. The energy analyzer has a slit lens and uses a two-dimensional detector. One dimension of this detector relates to the energy of the detected electron. The other dimension refers to where the electron entered the slit lens, i.e. the ϕ coordinate of Fig. 1. Recently the position of the electron gun was changed in such a way that the scattering angle is now 135°, (rather than 120° as described in Ref. [6]) and we report here on measurements in both configurations. For the new scattering geometry, incoming beam, sample surface normal and center of the analyzer (i.e. $\phi = 0$) are all in the same plane. The Si(001) samples

* Corresponding author.
E-mail address: maarten.vos@anu.edu.au (M. Vos).

0039-6028/$ – see front matter © 2010 Elsevier B.V. All rights reserved.
doi:10.1016/j.susc.2010.02.016

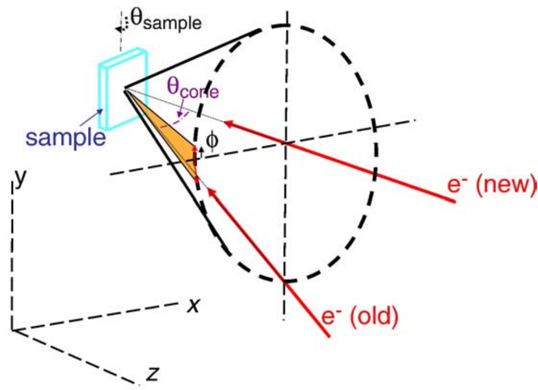

Fig. 1. A schematic view of the spectrometer geometry. Electrons that travel along the hatched part of the cone (half angle of the cone $\theta_{cone} = 44.3°$) are detected. Two electron gun orientations were used. In the old geometry the gun was in the *y–z* plane pointing upwards by 44.3° and the scattering angle was ≈120°. In the new geometry the electron gun is along the *z*-axis (= symmetry axis of the cone) and the scattering angle is 180 − 44.3 = 135.7°. The sample can be rotated about the vertical (*y*-) axis, and changing θ_{sample} affects the direction of the incoming and outgoing beams relative to the crystal.

were oriented such that the *(110)* plane was approximately horizontal. Thus for any value of θ_{sample} (see Fig. 1) a direction in the *(110)* plane was pointing towards the analyzer, and we can measure the corresponding Kikuchi band. The Al_2O_3(0001) sample was aligned such that the *(1110)* Kikuchi band was always visible in the analyzer.

During the measurement the analyzer voltage is scanned in such a way that each position of the two-dimensional detector contributes equally to the spectrum at all energies. Thus the spectra obtained in this way are not distorted by variations in detector efficiencies of the two-dimensional detector. The same is not true for the angular distributions, as a specific position of the detector always contributes to the same ϕ angle. In order to obtain valid angular distributions we have to normalize the results for the varying detector efficiency. This is done by measuring the yield of a polycrystalline shim. Here no angular variations are expected and by taking the ratio of the crystal signal and shim signal one eliminates the contribution of the detector efficiency variation to the angular distribution. We will see that the shim signal can be replaced by that of a non-epitaxial over layer, or a randomly imbedded impurity.

3. Results

3.1. Xe in Si

In our laboratory we clean the Si crystal by sputtering with 2 keV Xe^+ ions, followed by a heat treatment using electron beam annealing. The sample temperature reached over 600 °C as was judged by its faint red glow. After such annealing, to remove the sputter damage, we still observe two distinct elastic peaks in the ERBS spectrum, as is evident in Fig. 2, (left panel). The separation of the two peaks is very close to the calculated separation of Si and Xe, suggesting some Xe is left in the sample after annealing. Quantification of the amount of Xe remaining in the sample would appear feasible by comparing the Xe elastic peak with the Si elastic peak. However the Xe signal strength (relative to the Si signal strength) depends on which part of the angular range of the detector is used to obtain the spectra. Spectra taken for $-1° < \phi < 1°$ appear to have a weaker Xe signal than those taken for $-3° < \phi < -2°$ and $2° < \phi < 3°$.To investigate the cause of this variation we plot the angular yield of the Si elastic peak, and Xe signal (Fig. 2, central panel). There is a clear structure in the Si yield. If we move the sample upwards, so the electron beam hits the supporting metal shim, rather than the Si crystal, and we measure the angular yield of the elastic peak of the shim, then we get a less-pronounced angular structure, also shown in the central panel of Fig. 2. This angular structure is due to the varying efficiency of the channel plates. Virtually the same angular distribution is found if we determine the angular variation in yield of the Xe inside the Si sample.

Dividing the Si yield by the shim yield (and hence removing the effect of varying detector efficiency) results in a rather symmetric distribution, with a maximum intensity near 0°. The observed intensity profile is attributed to a *(220)* Kikuchi band which always points into the direction of the analyzer when the oriented sample is rotated using the manipulator. The width of a Kikuchi band is approximately twice the Bragg angle: λ/D ($\lambda = 0.006$ nm for 40 keV e^-). For the *(220)* plane ($d_{220} = 0.192$ nm) twice the Bragg angle is 1.8°. This is in good agreement with the observed width ($2.8 sin 44.3° = 1.95°$) supporting this interpretation. See Ref. [11] for more details about the measurement of Kikuchi bands using our analyzer. Thus the presence of the Si Kikuchi band (and hence variations in the Si elastic peak yield) is the cause of the apparently different Xe levels in the spectra obtained from different angular ranges of the detector.

To get some insight in the surface sensitivity of these signal enhancement effects we measured the angular distribution directly

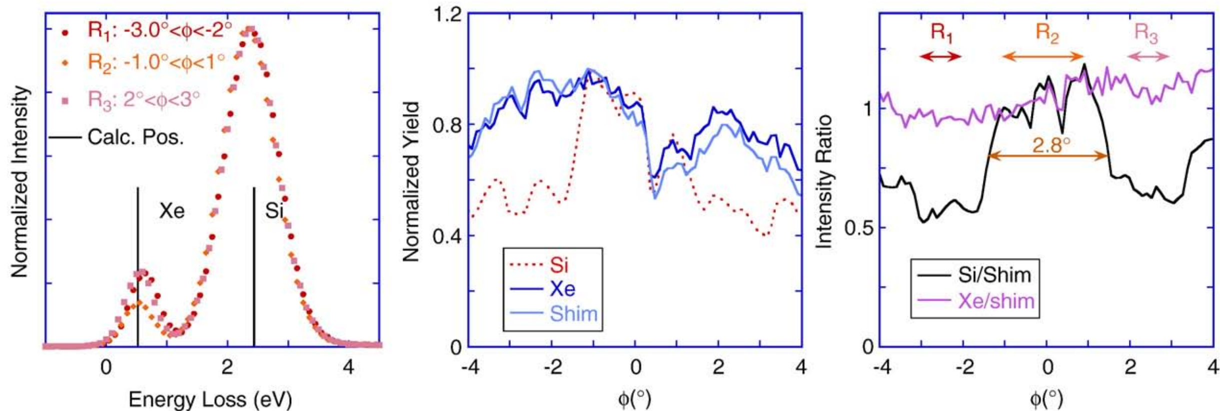

Fig. 2. The spectrum of a Xe-sputtered Si crystal after annealing (left panel). Spectra obtained from a different angular range of the detector are shown, all normalized to equal Si peak height. The main peak is aligned with the calculated peak position for 40 keV e^- scattering over 120° from Si. Using this energy scale the impurity peak lines up with the expected energy position of Xe. The relative Xe signal strength depends on the angular (ϕ) range of the analyzer used. The measured angular distribution for the Si elastic peak, Xe impurity and polycrystalline shim are shown in the central panel. The shim and Xe distributions are quite similar, but the Si distribution shows more structure. Dividing the Si yield by the shim yield shows a strong band (width 2.8°) of enhanced intensity near $\phi = 0$, whereas the normalized Xe intensity shows little structure. The different angular ranges used to obtain the spectra of the left panel are indicated by arrows.

after sputtering and after a complete sputter-anneal cycle. In this case we aligned the close packed [1$\bar{1}$1] direction with the analyzer. The spectra and the corresponding angular distributions are shown in Fig. 3. After sputtering and annealing a large enhancement of the Si peak is found in that direction, much more than the planar case shown in Fig. 2.

This variation of the intensity ratio is much larger than in the (Xe/Si) case described in the previous section, as there the Si signal enhancement was due to a single *(110)* plane pointing towards the detector. At the [1$\bar{1}$1] direction three *(110)*-type planes cross, and hence a much stronger enhancement of the Si intensity is expected.

If we measure the same direction after sputtering without an anneal treatment then we observe a larger Xe signal in the elastic peak spectra (indicating that the large fraction of the Xe desorbs during the annealing stage) but we still see a variation in intensity with angle, but this variation is only half as big as seen after subsequent annealing. These measurements probe thus the crystal order over a depth that exceeds the thickness of sputter-beam induced amorphized surface layer.

Based on an elastic scattering cross section σ_{elast} of 6.2×10^{-18} cm^2 as calculated using ELSEPA [12] we calculate for 40 keV e^- in Si an elastic mean free path of 322 Å ($\lambda_{\text{elast}}=1/n\sigma$ with n as the atom density). The mean range of 2 keV Xe in amorphous Si is 54 Å, with some ions reaching 100 Å [13] but in crystals, due to channeling, damage will extend to a larger depth. The sputter damage range is thus expected to be somewhat smaller than the elastic mean free path of the probing electrons. Hence, it is indeed expected that a sputtering-induced amorphisation of the near-surface layer causes a significant reduction of the Kikuchi line intensity.

3.2. Au on Si

A second example is a Si wafer on which ≈2 Å of Au was deposited straight after introducing it into the vacuum. The thickness was estimated using a crystal thickness monitor. Such a thin layer gives a strong signal in the ERBS spectrum, as the cross section of Au (due to its high atomic number) for elastic scattering is large. We aligned again the close packed [1$\bar{1}$1] direction with the analyzer. This causes a large enhancement of the Si peak in that direction and hence large variations in the Au:Si signal strength ratio. This is shown in Fig. 4. Experimentally the peak area ratio I_{Si}:I_{Au} varies from 1:0.4 (near [1$\bar{1}$1]) to 1:1.3 (away from [1$\bar{1}$1]).

As the Au is at the surface, its yield will not be affected by the underlying Si crystal structure. So the Au signal can be used as an internal reference of the analyser/detector efficiency as a function of angle. After division of the Si elastic peak yield by the Au yield we obtain the angular distribution shown in Fig. 4. This angular intensity

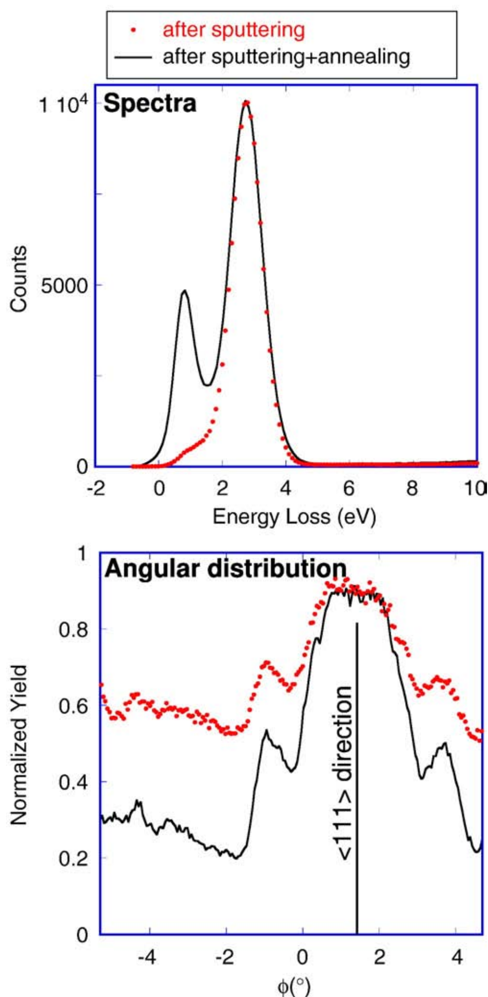

Fig. 3. The spectrum (top panel) and angular distribution (bottom panel) of a Si sample directly after sputtering with 2 keV Xe ions (dots) and after sputtering, followed by an anneal treatment (lines). The scattering angle was 135°, $E°$ 40 keV.

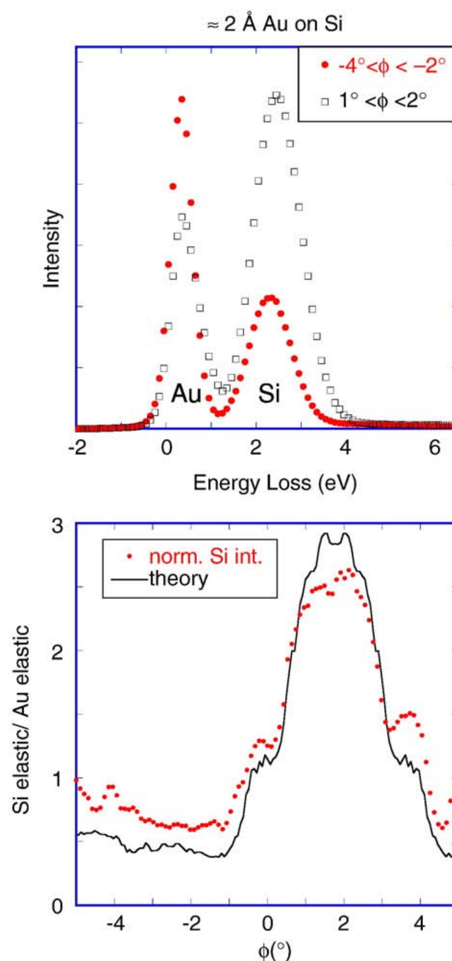

Fig. 4. Spectra of Au evaporated on Si for different angular ranges of the detector. Spectra are normalized to equal maximum height, the scattering angle was 120 and $E°$ 40 keV. Note the large variation of the Au to Si peak intensity ratio. The bottom panel shows the angular distribution of the ratio of the Si and Au signal strength. This ratio has a large peak near $\phi=2°$. Here the Si [111] crystallographic direction is pointing towards the analyzer resulting in an increase of the Si signal strength. As a comparison the calculated Si Kikuchi pattern is plotted as well for a line through the [111] direction. The good agreement indicates that the intensity variation of the spectra is indeed due to the Kikuchi pattern of the Si crystal.

distribution is in good agreement with the results obtained after sputtering and annealing and normalized using the shim data, as was shown in the previous section. Thus the 2 Å thick Au layer on top and the native oxide has little influence on the observed intensity distributions. Reasonable agreement is found as well with the theory of Winkelmann [14], also shown in this figure. Note that the maximum is slightly away from 0°. This indicates that the *(110)* plane of the crystal (containing the $[1\bar{1}1]$ direction) was not aligned perfectly in the horizontal direction.

3.3. Au on Al_2O_3

Finally we consider the case of Au on a sapphire (Al_2O_3) wafer. The wafer had a [0001] surface normal and was aligned with a *(1110)* horizontal measurement plane. Here things are even more complex as we distinguish three peaks in the ERBS spectra. One due to Au, one due to Al and one due to O. As is clear in Fig. 5 the calculated splitting of the three components is slightly larger than the observed one. This is not surprising as Al_2O_3 is a good insulator. The impinging electron beam will cause charging of the sample. This means that the energy of the impinging 40 keV electron beam is reduced by the charging potential, and the recoil energy is related to the actual energy of the beam in the sample, rather than the nominal energy outside the sample. From the results we estimate a charging of about 4 keV (for the 7 nA beam current used).

More interesting in the context of this paper is the large variation in shapes of both spectra. The Al signal is greatly enhanced relative to the O and Au signal, when rotating the sample by 1° from $\theta = 143°$ to $\theta = 144°$. This is also the case for the spectra corresponding to other ϕ intervals (not shown), and this suggests that Al and O are affected by incident and outgoing diffraction effects with different sensitivity. Unfortunately it is currently not possible to change the direction of the incoming beam without affecting the outgoing direction. So a firm experimental decoupling of the influence of the incoming and outgoing trajectories on the observed intensity distribution is currently not possible.

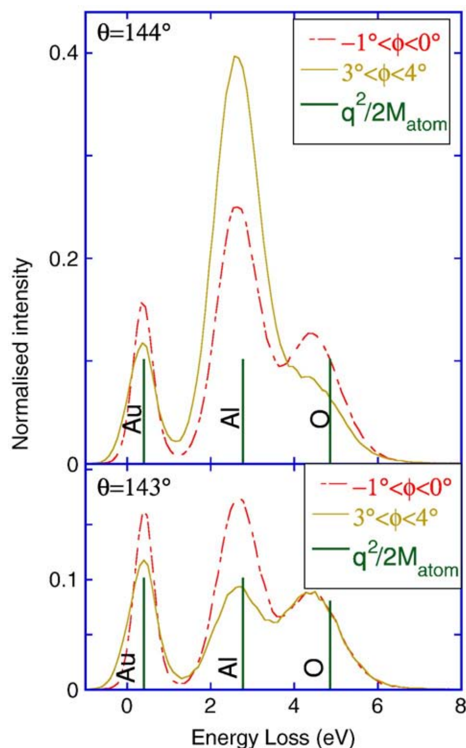

Fig. 5. Spectra of 0.6 Å Au on Al_2O_3. The scattering angle was 135°. The spectra shown were taken at two slightly different crystal orientations θ_{sample} and using different parts of the ϕ-range of the analyzer, as indicated. The expected separation (for 40 keV electrons) of the Au, Al and O peaks are indicated by the vertical bars. The area of the Au peak was normalized to unity for all four spectra. Note the large variation in the relative intensity of the different components.

4. Conclusion and discussion

In this paper we demonstrated that the crystal orientation can have large influences on the intensity ratio of different components of an ERBS spectrum. The reasonable agreement between theory and the current measurements seem to indicate that more careful experiments (more precise control of the sample orientation, and possible better quality of the surface) and improved theory (more diffracted beams included in the calculations, a better model for the thickness of the surface layer that contributes to these distributions) has the promise of more fully quantitative agreement between experiment and theory. These large variations in signal strength with orientation implies that the use of ERBS to determine the composition of single crystal surfaces is challenging, as a sub-degree accuracy of the crystal orientation required for quantitative work. In this context the 30% deviation of the the In:P signal intensity of InP wavers found in one of the earlier ERBS studies [15] is hardly surprising. The detail-rich structure of the angular distributions is, however, a good test of our capability to calculate Bloch functions accurately.

Similar Kikuchi band effects are known in core level photoelectron diffraction at lower energies [16,17], but the angular distributions show increasingly sharp structures with increasing energy [18]. This sets some limitations to the use of high-energy electrons for analysis of the near-surface area of single crystals as diffraction effects will have to be taken into account in fully quantitative analysis.

In principle one could overcome these problems by designing an analyzer with a very large opening angle. This would average out the angular intensity variations. Designing such an analyzer is far from trivial. The good energy resolution required for ERBS implies the use of fairly low pass energies ($E_{analyzer} = 200$ eV in our case). Thus the deceleration ratio in the lens stack is large (here 40000/200 = 200). The lens stack forms an image of the beam spot at the entrance of the hemispherical analyzer. This image is transferred to the detector by the hemispherical analyzer, and should not exceed the spatial resolution of the detector. The divergence of the electron beam entering the analyzer θ_a has to stay fairly small in order to prevent aberrations limiting the resolution. According to the Helmholtz–Lagrange equation:

$$A(E)\Omega(E)E = constant \quad (1)$$

with $A(E)$ the spot size, $\Omega(E)$ the solid angle of the electron beam at energy E. Both $A(E_{analyzer})$ and $\Omega(E_{analyzer})$ have maximum values, in order to have good analyzer performance. Thus $\Omega(E_{target})$ can only be made large if the beam spot $A(E_{target})$ is small.

We have found previously that diffracted ERBS intensity distributions can be simulated using a Bloch wave approach [11]. Thus if one has good control of the sample orientation then the measured intensity distributions can be corrected for the diffraction effects with the help of these simulations. Viewed differently, ERBS combined with diffraction can also provide information on the real-space structure of the sample, potentially with chemical sensitivity based on the recoil effect.

Experiment and theory will only agree if the calculated Bloch functions are a good approximation of actual electron wave function. Thus for a known sample structure these measurements provide a unique fingerprint of the Bloch function of keV electrons.

Acknowledgement

We want to thank Les Allen and Erich Weigold for stimulating discussions, Almamun Ashrafi for providing us with an oriented sapphire wafer. This research was made possible by a grant of the Australian Research Council.

References

[1] M. Vos, Phys. Rev. A 65 (2002) 12703.
[2] F. Yubero, V.J. Rico, J.P. Espinos, J. Cotrino, A.R. Gonzalez-Elipe, Appl. Phys. Lett. 87 (2005) 084101.
[3] D. Varga, K. Tokési, Z. Berényi, J. Tóth, L. Kövér, Surf. Interface Anal. 38 (2006) 544.
[4] M. Filippi, L. Calliari, Surf. Interface Anal. 40 (2008) 1469.
[5] M. Went, M. Vos, Appl. Phys. Lett. 90 (2007) 072104.
[6] M. Vos, M. Went, Nucl. Instrum. Meth. B 266 (2008) 998.
[7] G. Gergely, Prog. Surf. Sci. 71 (2002) 31.
[8] J.A. Venables, C.J. Harland, Phil. Mag. 27 (1973) 1193.
[9] A.J. Schwartz, M. Kumar, B.L. Adams, D.P. Field (Eds.), Electron Backscatter Diffraction in Materials Science, Springer, 2009.
[10] D.C. Joy, D. Newbury, D. Davidson, J. Appl. Phys. 53 (1982) R81.
[11] M. Went, A. Winkelmann, M. Vos, Ultramicroscopy 109 (2009) 1211.
[12] F. Salvat, A. Jablonski, C.J. Powell, Comput. Phys. Commun. 165 (2005) 157.
[13] J. Ziegler, J. Biersack, U. Littmark, The Stopping and Range of Ions in Solids, Pergamon Press, New York, 1985.
[14] A. Winkelmann, C. Trager-Cowan, F. Sweeney, A.P. Day, P. Parbrook, Ultramicroscopy 107 (2007) 414.
[15] M. Went, M. Vos, R.G. Elliman, J. Electron Spectrosc. Relat. Phenom. 156–158 (2007) 387.
[16] O. Küttel, R. Agostino, R. Fasel, J. Osterwalder, L. Schlapbach, Surf. Sci. 312 (1–2) (1994) 131.
[17] T. Katayama, H. Yamamoto, Y.M. Koyama, S. Kawazu, M. Umeno, Jpn. J. Appl. Phys. 38 (1999) 1547.
[18] A. Winkelmann, C.S. Fadley, F.J. de Abajo, New J. Phys. 10 (11) (2008) 113002.